Tellus (2005), 57B, 70–86
Printed in UK. All rights reserved

TELLUS

The oceanic response to carbon emissions over the next century: investigation using three ocean carbon cycle models

By A. CHUCK[1]*, T. TYRRELL[2], I. J. TOTTERDELL[3]† and P. M. HOLLIGAN[2], [1]*School of Environmental Sciences, University of East Anglia, Norwich NR4 7TJ, UK;* [2]*School of Ocean and Earth Sciences, Southampton Oceanography Centre, University of Southampton, European Way, Southampton SO14 3ZH, UK;* [3]*George Deacon Division, Southampton Oceanography Centre, European Way, Southampton SO14 3ZH, UK*

(Manuscript received 29 October 2003; in final form 21 June 2004)

ABSTRACT

A recent study of coupled atmospheric carbon dioxide and the biosphere (Cox et al., 2000, *Nature,* **408**, 184–187) found alarming sensitivity of next-century atmospheric pCO_2 (and hence planetary temperature) to uncertainties in terrestrial processes. Here we investigate whether there is similar sensitivity associated with uncertainties in the behaviour of the ocean carbon cycle. We investigate this important question using three models of the ocean carbon cycle of varying complexity: (1) a new three-box oceanic carbon cycle model; (2) the HILDA multibox model with high vertical resolution at low latitudes; (3) the Hadley Centre ocean general circulation model (HadOCC). These models were used in combination to assess the quantitative significance (to year 2100 pCO_2) of potential changes to the ocean stimulated by global warming and other anthropogenic activities over the period 2000–2100. It was found that an increase in sea surface temperature and a decrease in the mixing rate due to stratification give rise to the greatest relative changes in pCO_2, both being positive feedbacks. We failed to find any comparable large sensitivity due to the ocean.

1. Introduction

1.1. Characterization of ocean uncertainties

Uncertainties in the response of *terrestrial* vegetation and respiration to climate change lead to uncertainties in atmospheric pCO_2 at 2100 of up to 250 ppm (Cox et al., 2000). This uncertainty is large compared with the "most likely" increase over the next 100 yr (about 350–400 ppm, from ∼360 today to ∼700–750 ppm at year 2100 (IPCC, 2001)), which makes estimates of future global warming much less well constrained. It is critical for society to be aware of such uncertainty in order to plan appropriately for worst-case contingencies as well as greatest-probability scenarios. In their high-resolution general circulation model (GCM), Cox et al. (2000) included a dynamic ocean and also a dynamic terrestrial biosphere, both of which were allowed to change in response to changing CO_2 and climate. They found that two feedbacks in particular (a large temperature influence on the rate of respiration of soil carbon and drying out of the Amazon rainforest), both terrestrial, made a large difference to year 2100 atmospheric pCO_2. This study is related, but not directly comparable, to that of Cox et al. (2000). Whereas Cox et al. (2000) explored only one scenario, and therefore only one set of assumptions about the nature and magnitude of each feedback, in this study we explore ocean feedbacks individually and adopt extreme assumptions about each feedback in order to assess the bounds to our uncertainty. Cox et al. (2000), with their one scenario, identified an alarmingly large dependence of year 2100 pCO_2 on uncertainties in future behaviour of the terrestrial biosphere. Here we take three models of the ocean carbon cycle and use them in a targeted way specifically to see if there is a similar degree of sensitivity due to uncertainties about future ocean behaviour.

1.2. Quantitative models

The impact of anthropogenic perturbations on the Earth system over the next 100 yr cannot be foretold with absolute certainty but can be estimated using models. At the lower end of complexity are box models, which range from simple two-box models, first suggested by Craig (1957), to multibox models such as the high-latitude diffusion–advection model (HILDA) used by Siegenthaler and Joos (1992). More recently, 3-D ocean general circulation models (OGCMs) such as the Princeton 3-D model

*Corresponding author.
e-mail: a.chuck@uea.ac.uk
†Now at: Met Office, Fitzroy Road, Exeter, Devon EX1 3PB, UK.

(Sarmiento et al., 1992), the Hamburg 3-D model (Maier-Reimer et al., 1993) and the Hadley Centre OGCM (HadOCC) (Cox et al., 2000) have been used. Recent modelling studies have investigated the effect of increasing CO_2 and climate change on ocean carbon cycling (Klepper and de Haan, 1995; Maier-Reimer et al., 1996; Sarmiento et al., 1998; Matear and Hirst, 1999; Joos et al., 1999; Plattner and Marchal, 2001; Bopp et al., 2001). These models, with the exception of that of Klepper and de Haan (1995) and Plattner and Marchal (2001), consider only simple changes in biological productivity (i.e. those driven by changes in circulation) but do not, for example, consider changes in external nutrient supply or species composition (IPCC, 2001). Klepper and de Haan (1995) used a 2-D global model of ocean chemistry and biology to investigate the sensitivity of oceanic CO_2 uptake to alterations of phytoplankton production due to CO_2 increase, increased UV radiation and eutrophication, in addition to temperature increase and decreasing circulation. Plattner and Marchal (2001) have examined scenarios of increasing and decreasing calcium carbonate producers. Here, we follow a similar approach to Klepper and de Haan (1995) but we assess the quantitative sensitivity of CO_2 accumulation in the atmosphere to ocean processes using three models of varying complexity: a new three-box model, the multibox model HILDA and the OGCM, HadOCC. We explore in greater depth the sensitivity of CO_2 accumulation to alterations in biological oceanographic processes, in addition to the physical changes associated with global warming. The importance of biological oceanographic processes to climate change has previously been questioned by Broecker (1991) with replies by Sarmiento (1991) and Longhurst (1991); in this paper we estimate the sensitivity to both biological and abiological feedbacks.

The steady-state models were forced with anthropogenic CO_2 emissions data for 1850 to 1990 and simulated emissions for 1990 to 2100 (Enting et al., 1994). The models were applied to investigate the possible changes in ocean functioning over the period 2000–2100 in response to various anthropogenic effects and to assess the extent to which these effects could exacerbate or ameliorate global warming. In the interests of brevity, we refer to these anthropogenic effects as "feedbacks" throughout. However, in some cases (e.g. increased fertilizer run-off into the ocean) the term is strictly incorrect because an induced change in atmospheric CO_2 does not feed back to alter the initial cause.

2. Model descriptions

We use three independently constructed models in this study, but give greater attention to explaining and validating the simplest model because, unlike the other two, it has not been previously published elsewhere.

2.1. The three-box model

The three-box model was developed from a two-box model of the oceanic nitrogen and phosphorus cycles (Tyrrell, 1999). This model includes three vertically stacked boxes: a surface box (0–100 m) which represents the euphotic zone, a middle box (100–500 m) which represents the annually mixed surface layer above the seasonal thermocline, and a deep box (500–3730 m) representing the deep layer below the annual thermocline. The model represents an average water column down to the sea bed, has a spatially and temporally averaged input of nutrients, carbon and alkalinity and does not take into account any latitudinal or horizontal variations. Phosphate is used as the limiting nutrient for primary productivity, in keeping with other geochemical models as it is thought to be the ultimate limiting nutrient (Tyrrell, 1999), although nitrogen could equally well have been used for this timescale. The biology is modelled explicitly, with the relevant parameters being taken directly from Tyrrell (1999). The carbon chemistry follows Lewis and Wallace (1997). The addition of a third box makes it possible to model both air–sea gas exchange and mixing with the deep box correctly. Differences between the depth profiles of $CaCO_3$ dissolution and of organic matter remineralization are also easier to represent with three boxes.

A potentially serious omission from the three-box model is the solubility pump. This meant that absolute pCO_2 values could not be calculated accurately; however, relative changes could be evaluated successfully. The intercomparison of the three models in this study enabled the effect of this omission to be evaluated.

A recognized deficiency in most older models is the omission of the calcium carbonate ($CaCO_3$) cycle, e.g. the models of Khesghi et al. (1991), Prentice et al. (2001), Shaffer (1993) and Yamanaka and Tajika (1996). One of our aims with this model was to model explicitly the cycling of $CaCO_3$ in order to assess the impact of potential changes to abundance of calcium carbonate-producing organisms such as coccolithophores.

2.1.1. Components of the three-box model. The distribution of CO_2 within the ocean is governed by physical, chemical and biological processes: the exchange of CO_2 between the atmosphere and the ocean, vertical and horizontal advection of water, the organic carbon and calcium carbonate pumps and chemical speciation.

(1) Distribution of total CO_2 (TCO2). Many processes together determine the distribution of TCO2. Processes represented in the model are: air–sea gas exchange of CO_2, riverine input of dissolved inorganic carbon, biological uptake of CO_2 into biomass, remineralization and burial of biomass, precipitation and dissolution of $CaCO_3$ and mixing processes between the three layers.

(2) Distribution of alkalinity. The important processes governing the distribution of alkalinity in the ocean (and in the model) are: riverine input of bicarbonate and nitrate, precipitation of $CaCO_3$ by organisms and the biological uptake of nitrate, the dissolution $CaCO_3$ deeper in the ocean and the remineralization of nitrate, burial of $CaCO_3$ and nitrate in biomass and mixing processes between the three layers.

The production of $CaCO_3$ in the surface ocean is linked to the production of organic matter through the "rain ratio" (RR), which is the molar ratio of $CaCO_3$ C export from the surface box to particulate organic carbon (POC) C export. This model also uses a "production ratio" (PR), which is the ratio of $CaCO_3$ production to total primary production, both in units of moles of C.

Processes that have been ignored in the model are the dissolution of $CaCO_3$ from the sediments and adjustment of the lysocline depth which occurs over a timescale of thousands of years (Sundquist, 1986) and the processes of nitrogen fixation and denitrification. Nitrate has only a small effect on alkalinity compared with the cycling of $CaCO_3$.

2.1.2. Model equations. The distribution of CO_2(aq) (dissolved inorganic carbon in the form of dissolved CO_2 gas, as opposed to bicarbonate or carbonate ions) within the ocean is a function of temperature, salinity, pressure, alkalinity and TCO2. The equations used to model alkalinity and TCO2 were formulated using the equations given by Sarmiento (1992):

$$\mathrm{SMS_{alkalinity}} = (2 \times \mathrm{SMS_{CaCO3}}) - \mathrm{SMS_N}$$
$$\mathrm{SMS_{TCO2}} = r_{\mathrm{C/P}}\mathrm{SMS_P} + \mathrm{SMS_{CaCO3}}$$

where SMS is "sources minus sinks" and $r_{C/P}$ is the Redfield ratio of carbon to phosphorus in organic matter. The cycling of nitrate is tied to the cycling of phosphate by Redfield ratios so SMS_N can be rewritten as $r_{N/P}$ SMS_P.

There are 11 variables in the model: phytoplankton biomass (B, phosphorus units) in the surface layer only; phosphate (P), TCO2 and alkalinity (A) in the surface, middle and deep layers; and atmospheric CO_2. The equations, parameter descriptions and values are shown in Appendices A and B. The differential equations were solved using a fourth-order Runge–Kutta algorithm (Press et al., 1992). Mass balance checks were carried out to verify that the total numbers of moles of phosphorous, carbon and total alkalinity were conserved in the system.

2.1.3. Initial model testing. The carbon cycle is presumed here to have been in steady state in pre-industrial times. The model is therefore arranged so that phytoplankton, phosphorus, carbon and alkalinity cycles are all in steady state before 1800, and so that the steady-state cycling is in reasonable agreement with literature estimates. Tables 1 and 2 show the model steady-state concentrations and steady-state global annual fluxes of carbon.

The pre-industrial steady state pCO_2 is assumed to be ~280 ppm (Watson et al., 1990). The atmospheric pCO_2 concentration produced by the model is 300 ppm, approximately 20 ppm too high. This small discrepancy is probably due to the omission of the solubility pump in this model.

2.1.4. Modelling the anthropogenic addition of CO_2 to the system. Carbon dioxide emission data for 1850–1990 were obtained from the Carbon Dioxide Information Analysis Center (CDIAC) (data available at http://cdiac.esd.ornl.gov/). These figures incorporated global CO_2 emissions from burning of fossil fuel, cement manufacture and gas flaring. To include emissions due to changes in land use 60% was added to the values, which kept the cumulative emissions similar to the IPCC value for the cumulative input of anthropogenic CO_2 (312 ± 40 Gt C during the period 1850 to 1986).

2.1.5. Modelling the "missing sink". This version of the model produces an atmospheric CO_2 concentration of 414 ppm in the year 1990, which, after correction for the missing solubility pump, is 394 ppm. However, the observed value in 1990 was 353 ppm (Keeling et al., 1996) i.e. the amount of anthropogenic carbon residing in the atmosphere is too high. The

Table 1. Three-box model steady-state concentrations[a]

Variable	Units	Model value	Literature values
Phytoplankton (standing stock)	mol P m^{-3}	1.37×10^{-5}	1.242×10^{-5} (Schlesinger 1997), 3.702×10^{-5} (Mackenzie et al., 1993), 1.851×10^{-5} (Goldman and Glibert, 1983), 1.415×10^{-5} (Barnes and Hughes, 1988)
Surface PO_4^{3-}	mol P m^{-3}	1.200×10^{-4}	0.743×10^{-4} (Takahashi et al., 1981), 0.15×10^{-4} (Craig et al., 1981)
Middle PO_4^{3-}	mol P m^{-3}	0.931×10^{-3}	2.045×10^{-3} (Takahashi et al., 1981), 0.4×10^{-3} (Craig et al., 1981)
Deep PO_4^{3-}	mol P m^{-3}	1.89×10^{-3}	2.201×10^{-3} (Takahashi et al., 1981), 1.85×10^{-3} (Craig et al., 1981)
Surface TCO2	mol C m^{-3}	2.021	2.041 (Takahashi et al., 1981), 2.005 (Craig et al., 1981)
Middle TCO2	mol C m^{-3}	2.149	2.224 (Takahashi et al., 1981), 2.075 (Craig et al., 1981)
Deep TCO2	mol C m^{-3}	2.281	2.308 (Takahashi et al., 1981), 2.270 (Craig et al., 1981)
Surface alkalinity	mol C m^{-3}	2.341	2.305 (Takahashi et al., 1981), 2.355 (Craig et al., 1981)
Middle alkalinity	mol C m^{-3}	2.358	2.325 (Takahashi et al., 1981), 2.340 (Craig et al., 1981)
Deep alkalinity	mol C m^{-3}	2.431	2.423 (Takahashi et al., 1981), 2.390 (Craig et al., 1981)
Atmospheric CO_2	ppm	300.5[b]	280 (Watson et al., 1990)

[a]All values given are for pre-anthropogenic concentrations.

[b]The model value for atmospheric CO_2 is too high due to the missing effect of the solubility pump.

Table 2. Three-box model steady-state carbon fluxes (Gt C yr^{-1})

Flux	Model value	Literature value
Total (net) primary production (TPP)	45.9	26.8 (Berger et al., 1987), 50 (Martin et al., 1987), 36.5–45.6 (Antoine et al., 1996), 45 (Mackenzie et al., 1993)
Sinking flux of POC at100 m	9.18	9.0 at 50 m (Yamanaka, 1995), 9.2 (Schlitzer, 1996)
Sedimenting flux of POC	0.24	0.44 (Schlitzer, 1996)
Riverine input flux of TCO2	0.43	0.389 (Ludwig et al., 1996), 0.4 (Wollast, 1994), 0.38 (Meybeck, 1993)
Air–sea flux of CO_2	0	−0.4 to −0.7 (Siegenthaler and Sarmiento, 1993)
Mixing flux into middle layer	1.72	?
Mixing flux into surface layer	10.12	?
Surface regeneration of POC	36.73	75–95% TPP = 34.5–43.7 (Appendix B)
Middle regeneration of POC	7.8	9.8% TPP = 4.5 (Appendix B)
Deep regeneration of POC	1.14	4% TPP = 1.84 (Appendix B)
Total production of calcite (TPC)	1.38	1.02 (Wollast, 1994), 1.0–2.0 (Shaffer, 1993), 0.63 (Milliman, 1993), 0.6 (Archer, 1996), 0.70 (Milliman et al., 1999)
Sinking flux of calcite at 100 m	1.38	0.42–0.75 (Sundquist, 1985), 1.2 (Schlitzer, 1996), 0.28 at 1000 m (Milliman, 1993)
Sedimenting flux of calcite	0.19	(Sundquist, 1985), 0.42 (Schlitzer, 1996), 0.204 (Wollast, 1994), 0.46 (Milliman 1993), 0.132 (Milliman et al., 1999)
Riverine flux of alkalinity	0.433	0.388 (Wollast, 1994); 0.44 (Sundquist, 1986)
Mixing flux into middle layer	0.96	?
Mixing flux into surface layer	45.91	?
Surface dissolution of calcite	0.0	0 (Wollast, 1994)
Middle dissolution of calcite	0.61	?
Deep dissolution of calcite	0.58	0.792 (Wollast, 1994), 0.49 (Broecker and Peng, 1982)

storage of this extra CO_2 has been termed the "missing sink" and is thought to be due to the greening of the Northern Hemisphere forests (Broecker and Peng, 1993). The dynamics of this extra sink (treeout) are poorly known and were incorporated into the model using a simple linear approach:

$$\text{treeout} = 0.01375 \times (p\text{CO}_2(\text{t}) - \text{pCO}_2(1800))$$

although a more complicated formulation was tried as a sensitivity analysis (see Section 5.2). Figure 1 shows that the value for atmospheric CO_2 at the end of the 300-yr run (1800–2100) is 744 ppm. In 1990, the corrected pCO_2 was 374 ppm which is still ∼20 ppm too high, but as the information available on the terrestrial sink is incomplete it was considered suitable for this model. This was used as the standard run of the three-box model.

2.2. HILDA

We used a version of the HILDA model (Shaffer and Sarmiento, 1995; Siegenthaler and Joos, 1992). This model has a single surface box for each of low-latitude and high-latitude regions, and a single mixed box for high-latitude deep water. The low-latitude deep ocean, in contrast, is represented with much higher vertical resolution, using a total of 68 stacked boxes. The model includes a separate overturning circulation in addition to mixing between adjacent boxes. We added explicit and dynamic phytoplankton and alkalinity to this model. Phytoplankton were simulated in the two surface boxes only; growth dependence on phosphate, maximum growth rate and phytoplankton mortality were identical to those used for the three-box model (Appendix B). The fraction of organic carbon that escaped remineralization in the surface layer (50% of the total) was remineralized down the water column using the Martin curve (Martin et al., 1987). The calcite flux was calculated as a multiple of the organic carbon flux (a forced rain ratio leaving the surface layer of particulate inorganic carbon (PIC):POC = 0.15). Fifty per cent of the calcite flux was remineralized in the upper water column (Milliman et al., 1999), using the Martin profile, the other 50% over a larger length scale.

2.3. HadOCC

We also carried out the perturbation experiments using the Hadley Centre ocean carbon cycle (HadOCC) model, a coupled physical–biogeochemical model of the ocean carbon cycle which is described fully in Palmer and Totterdell (2001). The HadOCC model was the ocean part of the GCM used by Cox et al. (2000) and so provides continuity with that study. The coarse-resolution version of the Hadley ocean model (HadOM3L) was used—this has a horizontal resolution of 3.75°E–W and 2.5°N–S and a vertical resolution of 10 m near the surface, increasing to 600 m at depth. The model was forced by climatological monthly means of surface and penetrating heat

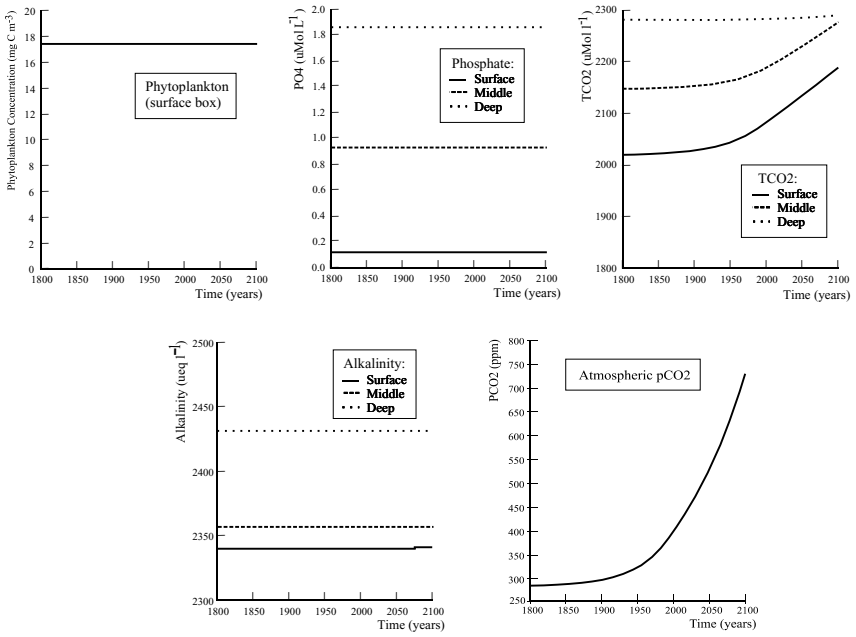

Fig 1. Model results for the standard three-box run.

fluxes, surface freshwater fluxes and wind stresses. There was also a very weak relaxation towards monthly means of sea surface temperatures and salinities. The forcing fields used were taken from the control run of the HadCM3 greenhouse gas experiment (Johns et al., 2003). The model was spun up for 100 yr, after which time the net air–sea flux was less than 0.1 Pg C yr^{-1} and biological production was stable.

3. Evaluation of the accuracy of the model results

3.1. The three-box model calibration and parameter justification

In order to apply the three-box model to various scenarios of anthropogenic perturbations, the model had to simulate the pre-industrial carbon cycle correctly. The steady-state model distributions of phosphate, alkalinity and TCO2 needed to agree with the estimated actual mean distributions of these variables in the global ocean prior to 1800. For the timescale under consideration (100 yr), it is the surface concentrations of these species that are most important. The greatest uncertainty in this model lies in the parametrization of the cycling of $CaCO_3$, as only a few major studies of this subject have been carried out (Milliman, 1993; Wollast, 1994; Milliman et al., 1999). The carbonate budget put forward by Milliman (1993) states that all the numbers used to compute the budget (apart from the input of calcium from rivers) are "subject to at least 25 to 50% uncertainty". In addition to keeping them close to literature estimates, the values of the parameters for calcite in the model were determined partly by the requirements of TCO2 and alkalinity long-term steady-state, and by tuning the model to reproduce the observed distribution of alkalinity in the ocean, according to the GEOSECS data (Craig et al., 1981).

The rain ratio—the ratio of the export rate of calcite to that of POC—is an important parameter in determining the surface partial pressure of CO_2 and was previously considered to be ∼0.25, i.e. 1 mole of calcite is exported for every 4 moles of POC (Broecker and Peng, 1982). However, the use of this value in calculating the production ratio in this model gave rise to alkalinity concentration gradients that did not agree with the gradients observed in the ocean, and which did not allow the model to reach a steady state. An analytical method (see Appendix C) was used to try to calculate the values of the parameters relating to the alkalinity distribution, namely the rain ratio, the dissolution parameters and the sedimenting fraction.

The steady-state production rate of biogenic $CaCO_3$ was 1.38 Gt C yr^{-1} using this model. This gave optimum values of 14% for the sedimenting fraction of calcite and 0.15 rather than 0.25 for the rain ratio. A $CaCO_3$ budget based on sediment traps, production estimates and sediment cores (Milliman, 1993) calculated the total production of calcite to be 0.63 Gt C yr^{-1}, with 60% of this sedimenting out. The total production estimate has since been revised to 0.69 Gt C yr^{-1} (Milliman et al., 1999). The total production of calcite produced in this model is two times higher than this, in line with values produced by other models: 1–2 Gt C yr^{-1} (Shaffer, 1993); 1.2 Gt C yr^{-1} (Archer and Maier-Reimer, 1994); 1.13 Gt C yr^{-1} (Wollast, 1994). Other estimates of the rain ratio have ranged from 0.10 to 0.28 (Shaffer, 1993; Yamanaka and Tajika 1996). Sarmiento et al. (2001) have recently estimated the global molar export ratio to

Table 3. Carbon uptake by the ocean, atmospheric and terrestrial reservoirs for the period 1980–1989

	Three-box model			HILDA			HadOCC		
Uptake	Ocean	Atmos.	Terr.	Ocean	Atmos.	Terr.	Ocean	Atmos.	Terr.
Gt C yr^{-1}	1.4	5.1	1.3	2.79	3.16	0.91	1.77	3.77	1.15
$\%CO_2$ emissions	17.6	66.1	16.3	41	46	13	26.5	56.4	17.2
Airborne fraction		0.7			0.5			0.6	

Table 4. Comparison of average oceanic uptake (Gt C yr^{-1})for the period 1980–1989 produced by carbon cycle models

Model name	Oceanic uptake rate (Gt C yr^{-1})
1-D box-diffusion model (Siegenthaler, 1983)	2.32
1-D three-box model (this study)	1.4
HILDA (Siegenthaler and Joos, 1992)	2.15
Princeton/GFDL[a]	2.2
MPI[a]	1.6
Hadley[a]	2.1
IPSL[a]	1.5
CSIRO (Matear and Hirst, 1999)	1.3

[a]Data taken from the Ocean Carbon-Cycle Model Intercomparison Project (OCMIP) (Orr et al., 2001).

be 0.06 ± 0.03, based on an ocean biogeochemical-transport box model and observations of the vertical gradients of potential alkalinity and nitrate.

For the model to reproduce the vertical distribution of alkalinity, a significant percentage of $CaCO_3$ underwent dissolution in the water column, with only 14% sedimenting out. Archer (1996), using a diagenetic model of $CaCO_3$ preservation in deep-sea sediments, predicted that 20–30% of the flux of $CaCO_3$ to the sea floor globally escapes dissolution. Milliman et al. (1999) provide evidence from a combination of box model, production and flux data, and laboratory feeding experiments that suggests that 40–80% of surface-produced carbonate is lost at depths shallower that 800–1000 m, and that only 20% is sequestered in deep-sea sediments.

3.2. Ocean uptake of CO_2

Table 3 shows the amount of carbon being taken up by the ocean, atmosphere and terrestrial reservoirs for the period 1980–1989 for the three-box model, the HILDA model and the HadOCC model. Table 4 shows estimates of the average oceanic CO_2 uptake rate (Gt C yr^{-1}) for the period 1980 to 1989 produced by other carbon cycle models.

The average uptake for this period has been estimated at 1.9 ± 0.6 Gt C yr^{-1} (IPCC, 2001). The three-box model produces an average uptake of anthropogenic CO_2 (no correction has been made for the natural pre-industrial efflux which is zero in this model) of 1.4 Gt C yr^{-1}. One would expect the CO_2 uptake to be slightly greater with the addition of the solubility pump. Ocean uptake rates derived from observational data are reported to be 1.5 ± 0.9 Gt C yr^{-1} for 1985 to 1995 (using the ocean ^{13}C inventory; Gruber and Keeling, 2001) and 1.8 Gt C yr^{-1} for 1980–1989 (using O_2 in firn air; Battle et al. 1996). The fossil fuel-induced rise in the oceanic dissolved inorganic carbon (DIC) inventory (standard run) differed between models. In HadOCC the amount of anthropogenic CO_2 that had found its way into the ocean rose from 128 Gt C at year 2000 to 450 Gt C at year 2100 (net anthropogenic air–sea flux at year 2100 was 4.00 Gt C yr^{-1}). The corresponding figures for the other two models are: HILDA model, 175 Gt C at 2000 to 675 Gt C at 2100 (6.40 Gt C yr^{-1} at 2100); three-box model, 94 Gt C at 2000 to 499 Gt C at 2100 (3.65 Gt C yr^{-1} at 2100).

4. Application of the models to anthropogenic perturbations

4.1. Perturbations to the system

To apply the models to predict the effects of global warming and the impact of possible feedback mechanisms in the ocean over the next 100 yr (2000–2100), the following tests were carried out.

4.1.1. Tests 1–3: Run-off of phosphate and nitrate fertilizers into the sea—simulating the anthropogenic effect of increased usage of fertilizers. Mackenzie et al. (1993) has estimated that the amount of phosphate added to freshwater and marine systems due to sewage and leaching of phosphate from fertilizers applied to the land is equal to 9×10^{10} mol P yr^{-1}. The amount of nitrate added via riverine input and atmospheric deposition is equal to 2×10^{12} mol N yr^{-1}. These figures are approximately double the amount being input in the model in the standard case for both species. The tests carried out were:

Test 1: Doubling the riverine input of phosphate to simulate the anthropogenic effect of increased usage of fertilizers.

Test 2: Doubling the riverine input of nitrate (its effect on alkalinity).

Test 3: Combining both of the above tests.

4.1.2. Tests 4–8: Increasing temperature—effects on solubility and growth rate. The temperature increase is projected to

reach on average 4 °C for the atmosphere and 1 °C for the sea surface during the next century (Mikolajewicz et al., 1990). Temperature has the ability to affect CO_2 solubility and carbonate chemistry; in addition, although not dealt with in this study, it might also lead to accelerated remineralization of dissolved organic carbon (Watson et al., 1990). The increase in temperature could lead to an increase in primary productivity.

Tests 2–6: increasing sea surface temperature by 1, 2 and 4 °C.

Tests 7 and 8: doubling the maximum growth rate of the phytoplankton and then combining this with the chemical effects of increased temperature.

4.1.3. Tests 9–12: Increasing temperature—effects on stratification. An increase in global temperature could potentially lead to an increase in stratification. The tests involved the following:

Tests 9–11: Halving the mixing rates between the surface and the middle, the middle and the deep layers and then both together.

Test 12: Combining the halving of both mixing rates with a 4 °C increase in sea surface temperature.

4.1.4. Tests 13–18: Changes in abundance of coccolithophores. To assess the likely role of calcifying organisms in influencing atmospheric pCO_2, tests were performed in which the amount of $CaCO_3$ produced was altered. There appear to be two conflicting ideas about the effect of increased concentrations of CO_2 on calcification. As anthropogenic CO_2 diffuses across the air–sea interface into the surface ocean, the pH drops. Growth experiments with coral reefs (Gattuso et al., 1998; Kleypas et al., 1999; Langdon et al., 2000) and coccolithophores (Riebesell et al., 2000) suggest that the lower pH impedes calcification. But in general, pelagic calcifying organisms appear to be more abundant in warmer climates (Holligan and Robertson, 1996) and so a global increase in sea surface temperature might also increase the abundance of calcifying organisms. To account for these alternative scenarios the following tests were carried out:

Tests 13–18: Changing the amount of calcite being produced by ±10%, ±30% and ±50%, i.e. changing the production ratio and therefore the rain ratio.

4.1.5. Tests 19–20: Changes in the strength of the biological pump. To explore further the role of biology in the uptake of anthropogenic carbon, the strength of the biological pump was altered by increasing (Test 19), or decreasing (Test 20), the efficiency of particle export. A greater (lesser) proportion of the particle flux was remineralized at depth, as opposed to near the surface. For instance, in a future climate scenario, diatoms could become the dominant phytoplankton species and so sinking speeds and therefore export efficiency would increase. Or, alternatively, in a warmer more stratified ocean, a more dominant recycling system would evolve.

Table 5 shows the relative increase/decrease in atmospheric pCO_2 in response to the perturbation tests.

5. Implications of model results

5.1. Influence of the feedback mechanisms

Climate change, resulting from a rise in global temperatures due to the addition of anthropogenic CO_2 to the atmosphere, could be modified by various feedback mechanisms, some relating to the functioning of the organic and inorganic carbon pumps and others to a change in ocean circulation. The tests performed on the models were considered to be plausible potential responses to global change. In each of the tests, the parameter under consideration was altered while the others were maintained at their reference values.

The short (100 yr) timescale considered in this work meant that the surface layer concentrations were the most significant. The deep layer concentrations remained unperturbed due to the long mixing time between the surface and deep ocean. It is important to remember that the values of atmospheric CO_2 concentrations resulting from the tests are slightly inaccurate (∼20 ppm too high) in the three-box model due to its set-up (i.e. the missing solubility pump), but in any case it is the relative changes in atmospheric CO_2 concentrations that are of interest in this study.

5.1.1. Tests 1–3: Run-off of phosphate and nitrate fertilizers into the sea. The first set of tests looked at the addition of phosphate and nitrate into the surface ocean as a result of fertilizer use. The tests involved doubling phosphate and nitrate separately and then jointly.

From the results in Table 5 it can be seen that all three tests resulted in a relatively small change in atmospheric pCO_2 (<3 ppm by 2100). The additional input of the limiting nutrient (phosphate in the three-box and HILDA models, nitrate in the HadOCC model) led to only a small increase in primary production. As the excess nutrient is utilized, the increase in growth results in a greater uptake of TCO2 and therefore a decrease in the partial pressure of CO_2 in the surface layer. This leads to a shift in equilibrium with the atmosphere such that more CO_2 is drawn down into the ocean to re-equilibrate.

The addition of nitrate affects alkalinity, but the contribution of nitrate to the alkalinity is small so only a slight change was observed. The addition of nitrate causes a decrease in alkalinity of the surface waters, leading to an increase in the partial pressure of CO_2 in the surface and so a net flux of CO_2 from the ocean to the atmosphere.

Combining the two tests led to an intermediate change in pCO_2, as would be expected. The effect of these tests was relatively small due to the residence time of many thousands of years for the two species in the ocean. The volume of river water entering the oceans each year (3.7×10^{13} m^3 yr^{-1}) is a thousand times less than the volume of the surface ocean (3.6×10^{16} m^3). River inputs are diluted upon entry to the ocean.

5.1.2. Tests 4–8: Increasing temperature—effects on solubility and growth rate. The second set of tests looked at the impact

Table 5. Response of the models to the perturbation tests

Test	Change in atmospheric pCO_2 at year 2100 compared with standard runs (ppm)					
	Three-box	HILDA	HadOCC	IPCC 'd'	Alt. terr. sink	K–deH[a]
Standard (ppm)	*747.1*	*634.1*	*700.5*	*597.8*	*956.1*	*785*
(1) Double RP	−2.8	−2.2	−0.4[b]	−2.7	−3.3	−3
(2) Double RN	+0.7	+0.5		+0.7	+0.5	
(3) Double RP & RN	−2.2	−1.7	−0.2[c]	−2.2	−2.7	
(4) Increase T by 1 °C[d]	+4.9	+8.3		+5.1	+6.8	
(5) Increase T by 2 °C[d]	+9.8	+16.6	+10.8[e]	+10.0	+13.7	
(6) Increase T by 4 °C[d]	+19.4	+33.3	+21.6[e]	+19.9	+27.4	+29
(7) Double max growth rate	−7.6	−35.2	−3.9[f]	−7.3	−11.6	+7[h]
(8) Double growth and increase T by 4 °C	+11.8	−1.9	+17.7[f]	+12.5	+16.1	
(9) Halve middle to surface mixing	+12.7	+22.6	N/A	+7.7	+19.0	
(10) Halve deep to middle mixing	+17.2	+10.7	N/A	+18.3	+16.3	+7[i]
(11) Halve both mixing coefficients	+25.1	+34.8	N/A	+19.0	+30.4	
(12) Halve both mixing and increase T by 4 °C	+40.4	+62.1	N/A	+35.2	+52.3	
(13) Decrease calcite by 10%	−1.9	−1.2		−1.7	−2.3	
(14) Decrease calcite by 30%	−5.8	−3.6		−5.3	−6.7	
(15) Decrease calcite by 50%	−9.7	−6.0	−4.3	−8.8	−11.0	−19[j]
(16) Increase calcite by 10%	+2.1	+1.2		+1.9	+2.0	
(17) Increase calcite by 30%	+6.0	+3.7		+5.6	+6.4	
(18) Increase calcite by 50%	+10.0	+6.1	+4.3	+9.2	+10.8	
(19) Increase export efficiency	−0.07	−4.0	−8.4[g]	−0.16	−0.2	
(20) Decrease export efficiency	−0.04	+12.3	+15.9[g]	−0.14	−0.2	

[a]Klepper and de Haan (1995).

[b]Extra nutrients are distributed evenly across the ocean surface, not at river mouths. There is no phosphate modelled in HadOCC. This run includes only the effect of extra nitrate on primary production.

[c]Includes both the effect of extra nitrate on production and the effect of extra nitrate on alkalinity.

[d]Due to non-linearities in the response of the CO_2 equilibrium chemistry to T change, a given increase in temperature will have a different effect depending on the starting temperature.

[e]The ocean surface temperature is relaxed to a value 4 °C higher everywhere. This results in reduced vertical transport near the surface (both diffusive mixing and vertical advection).

[f]Increase growth rate by 50% for HadOCC.

[g]Change sinking rate by ±25% for HadOCC.

[h] Warming also increases rates of phytoplankton mortality, respiration and excretion, and heterotrophic activity.

[i] Deep-water formation one-third of original value.

[j]Calcification is made proportional to saturation state.

of increasing temperature on the atmospheric CO_2 concentrations. Increasing temperature leads to higher atmospheric pCO_2 (maximum of 34 ppm by 2100 seen for HILDA), due to the warmer surface waters having reduced solubility for CO_2.

The increase in temperature could lead to an increase in primary productivity. This was simulated by doubling the maximum growth rate of the phytoplankton. Doubling the growth rate in the three-box model led to a decrease in atmospheric pCO_2 (−8 ppm at 2100) for the same reasons as doubling the input of phosphate, but the added effect of increased temperature overruled this and produced a net increase in atmospheric CO_2. A difference is seen in the effect of doubling the maximum phytoplankton growth rate in the three-box (8 ppm) and the HadOCC (4 ppm) models compared with the HILDA model (35 ppm) (see Section 5.2). For HILDA, the decrease in atmospheric pCO_2 caused by doubling the phytoplankton growth rate was greater than the increase in pCO_2 resulting from the increase in temperature.

5.1.3. Tests 9–12: Increasing temperature—effects on stratification. An increase in global temperature could potentially lead to an increase in stratification, so tests were carried out in which the mixing rates were lowered by 50%. Table 5 shows that out of all of the tests, changes in the mixing rate had the greatest impact on atmospheric CO_2 levels for the three-box model, with a 50% decrease in both surface and deep mixing rates causing a 25 ppm increase in atmospheric CO_2 at year 2100. Halving the deep to middle mixing rate produces a larger increase in pCO_2

than does halving the middle to surface mixing rate. This results from the decrease in surface alkalinity overriding the effect of higher primary production and decreased surface TCO2 in the former scenario. This model result shows how important it is to consider the vertical gradient in alkalinity as well as that of TCO2 when calculating the effects of changes in stratification. It was not possible to carry out comparable runs in HadOCC because mixing in this model is an emergent property rather than being imposed.

5.1.4. Tests 13–18: Changes in abundance of coccolithophores. To assess the likely role of calcifying organisms in influencing atmospheric pCO_2, tests were performed in which the amount of $CaCO_3$ produced was altered, both with 10, 30 and 50% decreases in calcite production and with 10, 30 and 50% increases in calcite production.

A decrease in $CaCO_3$ production of 50% would lead to a decrease in pCO_2 (-10 ppm by 2100) and an increase in $CaCO_3$ production to an increase in pCO_2 ($+10$ ppm by 2100) in the three-box model, with slightly smaller changes being seen in the HILDA and HadOCC models. A shift in ecosystem structure from organic or silica-walled organisms to carbonate-secreting organisms causes an increase in the surface water pCO_2. This is seen in Fig. 2 in which the surface concentrations of TCO2 and alkalinity for the three-box model runs with 50% increase and 50% decrease in $CaCO_3$ production are compared with the standard case.

5.1.5. Tests 19–20: Changes in the strength of the biological pump. To explore further the role of biology in the uptake of anthropogenic carbon, the strength of the biological pump was altered by increasing, or decreasing, the efficiency of particle export. For both these scenarios, very little change was seen in the atmospheric pCO_2 for the three-box model. With increased efficiency of export, primary production in the surface layer decreased due to less near-surface regeneration of nutrients, but the increase in pCO_2 that this should have produced appeared to be balanced by an increase in the surface alkalinity concentrations. With decreased export efficiency, the system jumped into a higher recycling mode, with the phytoplankton biomass increasing to a higher steady state but with no change in the TCO2 and alkalinity. The HILDA and HadOCC models both showed a decrease in pCO_2 with increasing export efficiency and an increase in pCO_2 (up to 16 ppm for HadOCC) for a decrease in export efficiency.

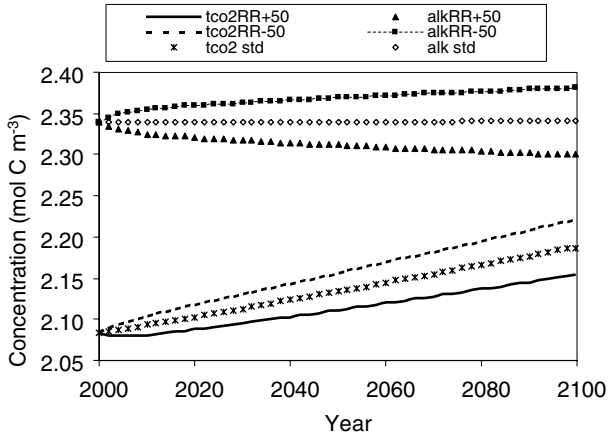

Fig 2. Effect of changing the rain ratio on surface concentrations of TCO2 and alkalinity.

In all these tests, the largest feedback effects are mostly positive (leading to higher atmospheric pCO_2 at year 2100) rather than negative. The large positive-feedback effects are also the most probable, such as the effect of increased temperature on dissociation constants and CO_2 solubility (runs 4–6), and the effects of global warming to increase stratification and decrease mixing (runs 9–12). The dominant influence of the physical, rather than the biological, feedbacks on the oceanic uptake of anthropogenic CO_2 has already been shown by several modelling studies (Klepper and de Haan, 1995; Maier-Reimer et al., 1996; Sarmiento and Le Quéré, 1996; Sarmiento et al., 1998; Matear and Hirst, 1999; Joos et al., 1999; Plattner and Marchal, 2001; Prentice et al., 2001). The studies by Sarmiento and Le Quéré (1996) and Sarmiento et al. (1998) suggested that changes in biology could modify the ocean carbon sink substantially, although they used the extreme scenarios of "abiotic" and "superbiota" to provide upper and lower limits for this effect. In this study, we have investigated what we consider to be more realistic scenarios of biological modifications. Only the major alterations, i.e. doubling the maximum growth rate or halving the calcification rate, resulted in effects on year 2100 pCO_2 of comparable magnitude to those caused by temperature and mixing.

5.2. Intercomparison of model results

Results from all three models concur in calculating that the likely impacts of anthropogenic changes to the ocean are small. Results from individual runs generally agree reasonably well between the three models. Where there are large differences these can be understood as follows:

(1) Increasing phytoplankton growth rate has a greater effect in the HILDA model than in the three-box model because HILDA has an extra surface box to represent high latitudes. There are surplus nutrients in this box, which are drawn down to a greater degree in this run. This effect is not seen to the same extent in HadOCC because of top-down control by zooplankton.

(2) Increasing export efficiency has a lesser effect in the three-box model, again because of the lack of low-latitude versus high-latitude distinction. In a high-nutrient surface box increasing export efficiency can lead to increasing drawdown of nutrients and carbon for the same rate of primary production. There is no such box in the three-box model, and in this case increasing export efficiency is counteracted by a decrease in primary production, because growth is nutrient-limited.

Where comparable runs were carried out, our results also agree well (in most cases) with those of Klepper and de Haan (1995) (see Table 5). However, in contrast to Klepper and de Haan (1995), one of the largest responses that we obtained was to a temperature-induced increase in phytoplankton growth rates in the HILDA model (∼35 ppm, Table 5). Out of the four models, therefore, the response of the HILDA model to doubled phytoplankton growth rates was much greater than that of any other model. The model of Klepper and de Haan (1995) in fact responded in the opposite direction from the other models. Although significantly higher than all the other models, HILDA's response might still be correct. The tendency of steady-state nutrients to be top-down (grazing) or bottom-up (nutrient) controlled is well known to be sensitive to the choice of parameter values and ecosystem structure (Frost and Franzen, 1992; Steele, 1992). Both the three-box and the HILDA models contain phytoplankton and phosphate as state variables, but do not explicitly model any zooplankton; zooplankton grazing is modelled implicitly as a 20% per day loss from the phytoplankton population. Nutrient and carbon drawdowns are therefore bottom-up controlled in these models, but only HILDA shows a response because the three-box model does not have a separate nutrient-rich high-latitude surface box.

In the HadOCC model, on the other hand, zooplankton (and detritus) are included as extra state variables. Therefore the zooplankton concentration can respond to changes in the phytoplankton growth rate: an increase in the latter causes (after a lag) an increase in the former, and so the grazing pressure on the phytoplankton also increases. A second factor is that increased chlorophyll in the surface waters means reduced illumination for phytoplankton lower in the water column. Because of these effects the primary production shows only a moderate increase, and not a doubling, when the growth rate is doubled, and similar responses are seen in the export production and the carbon drawdown. Therefore a smaller effect is seen than in the HILDA model.

The model of Klepper and de Haan (1995) model uses a quasi-steady-state approach, in which the components of the ecosystem are assumed to be always in equilibrium with each other and with the environment. Although the grazing pressure on the phytoplankton varies, there is no possibility of the phytoplankton escaping zooplankton control in this model. Much of the observed carbon drawdown in the North Atlantic is observed to occur during the spring bloom precisely when phytoplankton and zooplankton are decoupled, so this model may not be able to respond realistically to the doubling of the phytoplankton growth rate.

So which model is correct? The complexity of plankton ecosystems means that it is unclear how to represent them correctly in models. However, top-down control over nutrient drawdown has not yet been convincingly demonstrated for any oceanic regions, and so the HILDA model may well be the most realistic. These intermodel differences show the value of using more than one model.

5.3. *Sensitivity analyses*

All of the models contain simplifications, one or many of which may have affected the nature of our conclusions. To assess whether our conclusions are independent of some major model assumptions, we carried out the same tests in two variants of the three-box model.

(1) Political decisions, technological advances and other factors could lead to future emissions being very different from the IS92a scenario, and so we calculated the size of the different feedback effects using IPCC scenario (d) as the future CO_2 emission scenario (Enting et al., 1994), This gives a lower input of CO_2 into the atmosphere.

(2) There is major uncertainty in the future behaviour of the terrestrial biosphere as a source/sink for CO_2 and so our third sensitivity analysis examined whether the feedback effects were very different when a different scenario was used for the terrestrial biosphere response. In this analysis, the terrestrial biosphere becomes a source of CO_2 after 2040. An additional function was put into the model to represent the flux of CO_2 into the atmosphere due to soil respiration. This lagged the terrestrial uptake by 50 yr in order to simulate the lag in air temperature. The modelled terrestrial sink/source was adjusted to be comparable to that of Cox et al. (2000), who used a fully coupled, 3-D carbon-climate model to find that the terrestrial biosphere acts as an overall carbon sink until about 2050, after which it turns into a source, culminating in a source of ∼100 Gt C at 2100. The resulting pCO_2 obtained in the standard run of this model was 952 ppm which compares well with the 980 ppm obtained with the model of Cox et al. (2000).

Results of all the sensitivity analyses are shown in Table 5. It can be seen that the sign of each feedback effect is nearly always the same in each sensitivity analysis, and is generally of the same order of magnitude between variants of the three-box model.

5.4. *Greater uncertainty of terrestrial than of oceanic response*

Cox et al. (2000) whose GCM includes an explicit model of terrestrial vegetation (including soil respiration) coupled to the climate system, showed that atmospheric CO_2 may rise by 250 ppm more than generally expected. That result is due to a die-off of the Amazonian rainforest (caused by a shift in the geographical distribution of rainfall) and depends on assumptions of a levelling off of the CO_2 fertilization effect with increasing CO_2 and of a strong positive temperature response of respiration of organic matter on land. Even if their assumptions turn out to be partially incorrect (a similar run in another model (Friedlingstein et al., 2003) did not produce such a strong increase), it

is of interest in the context of this paper that no uncertainties of comparable magnitude have been seriously proposed for the ocean.

It is well understood that the ocean will continue to absorb a substantial fraction of the extra CO_2 that is being added to the atmosphere via diffusion across the sea surface, but this response is predictable and well understood. But beyond the straightforward diffusion of some of the excess CO_2 into the ocean, our model results suggest that the ocean is unlikely to hold any major surprises in terms of its ability to sequester CO_2 over the next century. The strongest effect we could find was of 62 ppm over the next 100 yr (Table 5), which is higher than the maximum effect of 29 ppm found by Klepper and de Haan (1995), also for the ocean, but about four times less than the 250 ppm found by Cox et al. (2000).

However, computer models are only as good as the assumptions and simplifications they contain and are by no means guaranteed to be definitive when simulating very complex systems (Oreskes et al., 1994). The short timescales considered may have curtailed the feedback effects such that ocean uncertainties will become more important over longer timescales. There could be significant oceanic feedbacks that we have missed because of insufficient imagination in postulating possible feedback responses. For instance, we did not include a sensitivity analysis of doubling the C:P ratio of organic matter because we could see no reason why such a large change should be produced by human activities. But if it were to occur then such a change could have a large effect on atmospheric pCO_2 (of the order of 100 ppm). Likewise we did not simulate a complete lifting of iron limitation in high-nutrient, low-chlorophyll (HNLC) regions, because such a drastic change to remote oceans seems unlikely; nor did we simulate the effects of increased or decreased carbon storage in the form of dissolved organic carbon (DOC) in the surface ocean. Time-series measurements of DOC in surface waters of the low-latitude Atlantic and Pacific (Lomas et al., 2002) suggest that extra DOC is accumulating there at a rate of $\sim$1.2 μmol kg^{-1} yr^{-1}. If true over the whole ocean and if maintained for the next 100 yr then this accumulation of DOC could reduce year 2100 atmospheric pCO_2 by 24 ppm. Although the effect is not enormous, this surprising recent observation makes the point that ocean biogeochemistry is by no means fully understood. Perhaps other (as yet unforeseen) advances in understanding, not included in this modelling study, could lead to larger uncertainties in the ocean carbon cycle than have been calculated here.

In the future there will probably be increased heating of, and freshwater input to, high northern latitudes, leading to weakening of the North Atlantic deep water (NADW) formation and the thermohaline circulation (THC). We have not fully evaluated the sensitivity of ocean carbon cycling to this feedback (although see Table 5, rows 11 and 12). Joos et al. (1999) examined this feedback in a low-order physical–biogeochemical climate model and found that weakening of the THC has a relatively small effect on future atmospheric CO_2 levels up to year 2100 (reduction of 2.9% by 2100), although a greater effect in future centuries. The size of the effect by 2100 will depend on the degree of NADW weakening/collapse occurring prior to 2100.

Our modelling has concentrated on processes occurring within the oceanic water column and has largely ignored processes and reservoirs within sea floor sediments. Warming of such sediments could lead to large-scale release of methane from methane hydrates, a potentially significant positive feedback on global warming (Brewer, 2000). Likewise, our model runs simulated the carbon cycle but not other climate-affecting processes within the ocean such as biogenic trace gas emissions (e.g. dimethylsulfide and organohalogens). We have focused on the consequences for atmospheric carbon, and have ignored other possible consequences of these alternative scenarios for human society and natural ecosystems.

6. Conclusions

Fossil fuel emissions have led to an accumulation of CO_2 in the atmosphere and will lead to further accumulation over the next century. We used three models (a three-box model, a multibox model and an OGCM) to carry out a focused investigation of possible modification of this accumulation by various anthropogenic effects on the ocean. Some of the anthropogenic effects were positive, i.e. they decreased ocean storage and so increased the amount left to accumulate in the atmosphere; some effects were negative and led to more CO_2 being absorbed by the ocean. Positive effects seem more likely than negative. Most importantly, none of the alterations we examined made any large difference to the predicted accumulation of CO_2 in the atmosphere. The largest effect is of the order of 60 ppm by the end of this century, which is small compared with the greater than 300 ppm rise in atmospheric CO_2 predicted over the same period, and small compared with a potential 250 ppm effect of uncertainties in terrestrial processes (Cox et al., 2000).

7. Acknowledgments

We are grateful to Fortunat Joos for code for the HILDA model, and to Bob Key and Chris Sabine for carbon chemistry routines. This paper benefited from comments by Jochem Marotzke, Andrew Yool, Andy Ridgwell and two anonymous reviewers. This work was partly funded by an UK Natural Environment Research Council fellowship (GT5/98/15/MSTB) to TT.

8. Appendix A: three-box model equations

Phytoplankton and phosphate concentrations are in units of moles P m^{-3}. TCO2 is in moles C m^{-3}, alkalinity is in moles of charge equivalents m^{-3} and atmospheric CO_2 is in parts per million (ppm).

$$\frac{\mathrm{d}B}{\mathrm{d}t} = \left(\mu_{\max}\frac{P_\mathrm{s}}{P_\mathrm{s}+P_\mathrm{H}} - M\right)B = B_{\mathrm{grow}} - B_{\mathrm{die}}$$

where

$$B_{\mathrm{grow}} = \mu_{\max}\left(\frac{P_\mathrm{s}}{P_\mathrm{s}+P_\mathrm{H}}\right)B$$

and

$$B_{\mathrm{die}} = M \times B.$$

$$\frac{\mathrm{d}P_s}{\mathrm{d}t} = \frac{\mathrm{RP}}{\mathrm{SD}} + \frac{K_{\mathrm{SM}}(P_\mathrm{m}-P_\mathrm{s})}{\mathrm{SD}} + (B_{\mathrm{die}} \times \mathrm{SRP}) - B_{\mathrm{grow}},$$

$$\begin{aligned}\frac{\mathrm{dTCO2_s}}{\mathrm{d}t} = {} & \left[\left(\frac{\mathrm{RC}+\mathrm{asg}}{\mathrm{SD}}\right) + (B_{\mathrm{die}} \times \mathrm{CP_{org}} \times \mathrm{SRC})\right. \\ & + \left(\frac{K_{\mathrm{SM}}(\mathrm{TCO2_m}-\mathrm{TCO2_s})}{\mathrm{SD}}\right) \\ & \left. - (B_{\mathrm{grow}} \times \mathrm{CP_{org}})\right] \\ & + [(B_{\mathrm{die}} \times \mathrm{CP_{org}} \times \mathrm{PR} \times \mathrm{SDCAL}) \\ & - (B_{\mathrm{grow}} \times \mathrm{CP_{org}} \times \mathrm{PR})]\end{aligned}$$

where asg equals air–sea gas exchange,

$$\begin{aligned}\frac{\mathrm{d}A_\mathrm{s}}{\mathrm{d}t} = {} & \left[\frac{\mathrm{RA}}{\mathrm{SD}} + \left(\frac{K_{\mathrm{SM}}(A_\mathrm{m}-A_\mathrm{s})}{\mathrm{SD}}\right)\right. \\ & + 2(B_{\mathrm{die}} \times \mathrm{CP_{org}} \times \mathrm{PR} \times \mathrm{SDCAL}) \\ & \left. - 2(B_{\mathrm{grow}} \times \mathrm{CP_{org}} \times \mathrm{PR})\right] \\ & - \left[\left(\frac{\mathrm{RN}+\mathrm{AN}}{\mathrm{SD}}\right) + (B_{\mathrm{die}} \times \mathrm{NP_{org}} \times \mathrm{SRP})\right. \\ & \left. - (B_{\mathrm{grow}} \times \mathrm{NP_{org}})\right]\end{aligned}$$

$$\begin{aligned}\frac{\mathrm{d}P_\mathrm{m}}{\mathrm{d}t} = {} & \left(B_{\mathrm{die}} \times \mathrm{MRP} \times \frac{\mathrm{SD}}{\mathrm{MD}}\right) \\ & + \left(\frac{K_{\mathrm{MD}}(P_\mathrm{d}-P_\mathrm{m})}{\mathrm{MD}}\right) - \left(\frac{K_{\mathrm{SM}}(P_\mathrm{m}-P_\mathrm{s})}{\mathrm{MD}}\right)\end{aligned}$$

$$\begin{aligned}\frac{\mathrm{dTCO2}_m}{\mathrm{d}t} = {} & \left[\left(B_{\mathrm{die}} \times \mathrm{CP_{org}} \times \mathrm{MRC} \times \frac{\mathrm{SD}}{\mathrm{MD}}\right)\right. \\ & + \left(\frac{K_{\mathrm{MD}}(\mathrm{TCO2_d}-\mathrm{TCO2_m})}{\mathrm{MD}}\right) \\ & \left. - \left(\frac{K_{\mathrm{SM}}(\mathrm{TCO2_m}-\mathrm{TCO2_s})}{\mathrm{MD}}\right)\right] \\ & + \left(B_{\mathrm{die}} \times \mathrm{CP_{org}} \times \mathrm{MDCAL} \times \mathrm{PR} \times \frac{\mathrm{SD}}{\mathrm{MD}}\right)\end{aligned}$$

$$\begin{aligned}\frac{\mathrm{d}A_\mathrm{m}}{\mathrm{d}t} = {} & \left[\left(2B_{\mathrm{die}} \times \mathrm{CP_{org}} \times \mathrm{PR} \times \mathrm{MDCAL} \times \frac{\mathrm{SD}}{\mathrm{MD}}\right)\right. \\ & \left. + \left(\frac{K_{\mathrm{MD}}(A_\mathrm{d}-A_\mathrm{m})}{\mathrm{MD}}\right) - \left(\frac{K_{\mathrm{SM}}(A_\mathrm{m}-A_\mathrm{s})}{\mathrm{MD}}\right)\right] \\ & - \left(B_{\mathrm{die}} \times \mathrm{NP_{org}} \times \mathrm{MRP} \times \frac{\mathrm{SD}}{\mathrm{MD}}\right)\end{aligned}$$

$$\frac{\mathrm{d}P_\mathrm{d}}{\mathrm{d}t} = \left(B_{\mathrm{die}} \times \mathrm{DRP} \times \frac{\mathrm{SD}}{\mathrm{DD}}\right) - \left(\frac{K_{\mathrm{MD}}(P_\mathrm{d}-P_\mathrm{m})}{\mathrm{DD}}\right)$$

$$\begin{aligned}\frac{\mathrm{dTCO2}_d}{\mathrm{d}t} = {} & \left[\left(B_{\mathrm{die}} \times \mathrm{CP_{org}} \times \mathrm{DRC} \times \frac{\mathrm{SD}}{\mathrm{DD}}\right)\right. \\ & \left. - \left(\frac{K_{\mathrm{MD}}(\mathrm{TCO2_d}-\mathrm{TCO2_m})}{\mathrm{DD}}\right)\right] \\ & + \left(B_{\mathrm{die}} \times \mathrm{CP_{org}} \times \mathrm{PR} \times \mathrm{DDCAL} \times \frac{\mathrm{SD}}{\mathrm{DD}}\right)\end{aligned}$$

$$\begin{aligned}\frac{\mathrm{d}A_\mathrm{d}}{\mathrm{d}t} = {} & \left[\left(2B_{\mathrm{die}} \times \mathrm{CP_{org}} \times \mathrm{PR} \times \mathrm{DDCAL} \times \frac{\mathrm{SD}}{\mathrm{DD}}\right)\right. \\ & \left. - \left(\frac{K_{\mathrm{MD}}(A_\mathrm{d}-A_\mathrm{m})}{\mathrm{DD}}\right)\right] \\ & - \left(B_{\mathrm{die}} \times \mathrm{NP_{org}} \times \mathrm{DRP} \times \frac{\mathrm{SD}}{\mathrm{DD}}\right)\end{aligned}$$

$$\frac{\mathrm{d}p\mathrm{CO_2}}{\mathrm{d}t} = (1\times10^6) \times \mathrm{asg} \times \frac{\mathrm{OA}}{\mathrm{AV}}.$$

9. Appendix B: three-box model parameter values

Symbol	Description	Units	Model value	Literature value
CP_{org}	Ratio of C:P in organic biomass		106	106 (Libes, 1992), 106 (Copin-Montegut and Copin-Montegut, 1983)
NP_{org}	Ratio of N:P in organic biomass		16	16 (Libes, 1992), 16–17 (Copin-Montegut and Copin-Montegut, 1983)
μ_{max}	Maximum growth rate of phytoplankton	yr^{-1}	0.25 d^{-1} = 91.25 yr^{-1}	0.1–4.1 d^{-1} (Furnas, 1990), 0.3–2.7 d^{-1} (Banse, 1982)
P_H	Michaelis–Menton half-saturation constant for growth versus PO_4	mol P m^{-3}	0.03×10^{-3}	0.03×10^{-3} (McAllister et al., 1964), 0.05×10^{-3} (Davies and Sleep, 1981)
M	Mortality	yr^{-1}	0.2 d^{-1}	0.25–1.2 d^{-1} (Banse, 1992)
K_{SM}	Mixing coefficient between surface and middle layers	m yr^{-1}	18.25	15.76 (Munk, 1966)
K_{MD}	Mixing coefficient between middle and deep layers	m yr^{-1}	3.0	3.0 (Broecker and Peng, 1982), 1.0–5.0 (Sundquist, 1985)
SFP	Fraction of TPP incorporated into sediments	%	0.2	0.2 (Jahnke, 1992), 0.2 (Schlesinger, 1997), 0.1–0.2 (Mackenzie et al., 1993)
SRP	Fraction of TPP regenerated in the surface layer (0–100 m)	%	85	75–95 (Barnes and Hughes, 1988), 86 (Schlesinger, 1997), 85 (Martin et al., 1987), 90 (Berger et al., 1987)
MRP	Fraction of TPP regenerated in the middle layer (100–400 m)	%	12	9.8 (Martin et al., 1987), 9.0 (Schlesinger, 1997)
DRP	Fraction of TPP regenerated in the deep layer (400 m+)	%	2.8	3.7 (Martin et al., 1987)
SFC	Fraction of POC incorporated into sediments	%	0.5	
SRC	Fraction of POC regenerated in the surface layer (0–100 m)	%	80	
MRC	Fraction of POC regenerated in the middle layer (0–400 m)	%	17	
DRC	Fraction of POC regenerated in the deep layer (400 m+)	%	2.5	
SC	Fraction of calcite sedimented	%	14	46 (Milliman, 1993), 21 (Morse and Mackenzie, 1990), 34 (Wollast, 1994)
SDCAL	Fraction of calcite remineralized in the surface layer	%	0	?
MDCAL	Fraction of calcite remineralized in the middle layer	%	44	?
DDCAL	Fraction of calcite remineralized in the deep layer	%	42	?
RR	Rain ratio used to calculate production ratio		0.15	0.25 (Broecker and Peng, 1982), 0.08–0.12 (Yamanaka and Tajika, 1996)
RP	Riverine input of PO_4^{3-}	mol P m^{-2} yr^{-1}	0.2×10^{-3}	0.089×10^{-3} (Meybeck, 1993), 0.19×10^{-3} (Mackenzie et al., 1993)
RC	Riverine input of DIC	mol C m^{-2} yr^{-1}	0.1	0.0914 (Wollast, 1994), 0.09 (Ludwig et al., 1996)
RA	Riverine input of alkalinity	mol eq m^{-2} yr^{-1}	0.09	0.074 (Ludwig et al., 1996), 0.090 (Wollast, 1994), 0.089 (Meybeck, 1993)

B1. Continued

RN	Riverine input of nitrate	mol eq m^{-2} yr^{-1}	5.5×10^{-3}	(2.57–6.9)$\times 10^{-3}$ (Mackenzie et al., 1993), 2.83×10^{-3} (Meybeck, 1993), (2.77–6.9)$\times$ 10^{-3} (Cornell et al., 1995)
AN	Atmospheric deposition of nitrate	mol eq m^{-2} yr^{-1}	7.0×10^{-3}	5.94×10^{-3} (Duce et al., 1991), (2.77–6.92)$\times$ 10^{-3} (Cornell et al., 1995), (4.5–11.0)$\times$ 10^{-3} (Jaffe, 1992)
Symbol	Description	Units	Model value	Literature value
TEMP	Temperature	°C	18	18 (Levitus, 1982)
SAL	Salinity	psu[a]	35	35 (Levitus, 1982)
SD	Depth of surface layer	m	100	
MD	Depth of middle layer	m	300	
DD	Depth of deep layer	m	3330	
OA	Area of ocean surface	m^2	3.61×10^{14}	
AV	Volume of dry air in atmosphere	mol	1.8×10^{20}	
K_w	Piston velocity	m yr^{-1}	4.65	4.65 (Watson et al., 1991)

[a]psu, practical salinity unit.

(1) The following relationships were used to convert units if the ones stated are different from those in the literature: organic matter has the Redfield ratio of 106C:16N:1P; the relative molecular masses of the elements C, N and P are 12, 14 and 31 g respectively.

(2) The SF (%) depends on the value of TPP. To get an estimate of SF, the literature estimates of permanent burial were divided by a TPP of 46.05 Gt C yr^{-1} (Tyrrell, 1999).

(3) Estimates of the riverine inputs of phosphorus, carbon and alkalinity quoted just considered the dissolved forms. The parameters used were increased slightly to take into account the possibility that some of the particulate load might be available for use by the biota.

(4) The Michaelis–Menten half-saturation constant for a nutrient is the concentration of that nutrient at which either the growth rate or the nutrient uptake rate for the species consuming it is half of its maximum value. The literature values given in the table are for nutrient uptake whereas the model value is for growth because Droop kinetics are not modelled (Tyrrell, 1999).

10. Appendix C: parameterization of alkalinity

The inputs affecting alkalinity in the ocean are the riverine input of bicarbonate (RA) and the riverine (RN) and atmospheric (AN) inputs of nitrate. The outputs are the sedimenting out of calcite and of nitrate in organic matter. At steady state inputs equal outputs. In reality, glacial–interglacial variations of alkalinity implicated in temperature changes mean that the ocean may at the present time not be quite at steady state; however, for simplicity, we have assumed for this model that it is at steady state. Figure 3 shows a representation of the steady-state balance of the inputs and outputs of alkalinity.

Using the model parameters, the inputs of alkalinity (river input of bicarbonate minus river and atmospheric input of nitrate) sum to 31.6×10^{12} mol eq yr^{-1}. The output of alkalinity (2 $\times$ burial of calcite minus burial of nitrate) should therefore be equal to 31.6×10^{12} mol eq yr^{-1} and as the burial of nitrate can be calculated from the sedimenting fraction (SFP) multiplied by the primary productivity (TPP_N), the required burial of calcium carbonate can be found:

$$\begin{aligned}\text{Inputs} &= (\text{RA} - \text{RN} - \text{AN}) \times \text{ocean area}\\ &= [0.1 - (5.5 \times 10^{-3})\\ &\quad - (7.0 \times 10^{-3})] \text{ mol eq m}^{-2}\text{ yr}^{-1}\\ &\quad \times (3.61 \times 10^{14})\\ &= 31.6 \times 10^{12} \text{ mol eq yr}^{-1}.\end{aligned}$$

$$\text{Output} = (2 \times \text{TPC} \times \text{SC}) - (\text{TPP}_N \times \text{SFP})$$

$$\begin{aligned}\text{TPP}_N \times \text{SFP} &= 5.776 \times 10^{14} \text{ mol N yr}^{-1} \times 0.002\\ &= 1.16 \times 10^{12} \text{ mol N yr}^{-1}\\ &= 1.16 \times 10^{12} \text{ mol eq yr}^{-1}.\end{aligned}$$

Since input is equal to output:

$$31.6 \times 10^{12} = (2 \times \text{TPC} \times \text{SC}) - (1.16 \times 10^{12})$$

$$\text{TPC} \times \text{SC} = 16.4 \times 10^{12} \text{ mol C yr}^{-1}.$$

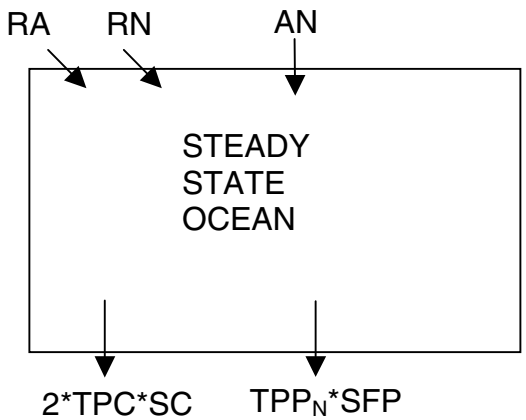

Fig 3. Representation of the steady-state balance of the inputs and outputs of alkalinity.

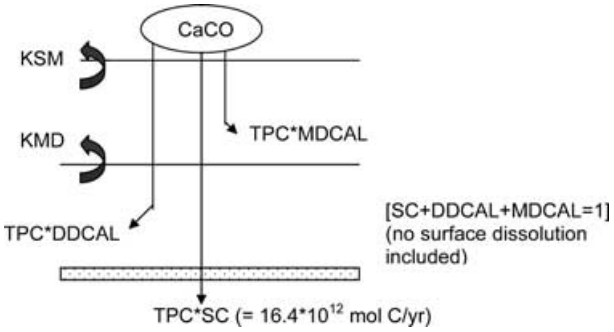

Fig 4. Internal processes governing the alkalinity gradient between the surface and deep layers in the ocean.

Figure 4 shows the internal processes governing the alkalinity gradient between the surface and deep layers in the ocean.

The concentration gradients for alkalinity observed in the real ocean are approximately 17 μeq l^{-1} between the surface and middle layers and $\sim$100 μeq l^{-1} between the surface and deep layers with the concentration increasing with increasing water depth. There is no homeostatic mechanism in the model controlling the concentrations of alkalinity (which there is for phosphate) so the steady-state balances needed to be worked out. The surface to deep gradient obtained in the model was made to equal the observed gradient in the real ocean by tuning the total production of calcite (TPC). This allowed the sedimenting fraction (SC) to be calculated (tuned) knowing that TPC $\times$ SC $= 16.4 \times 10^{12}$ mol C yr^{-1}. Using TPC/TPP$_C$ to get the production ratio, the rain ratio could be found using eq. (6). Realistic alkalinity gradients were produced in this way by tuning TPC and SC to values of 1.17×10^{14} mol C yr^{-1} and 14% respectively and this in turn led to a rain ratio of 0.15. These values are compared with the literature in Section 3.

References

Antoine, D., André, J.-M. and Morel, A. 1996. Oceanic primary production, 2. Estimation at global scale from satellite (Coastal Zone Colour Scanner) chlorophyll. *Global Biogeochem. Cycles* **10**, 57–69.

Archer, D. E. 1996. A data-driven model of the global calcite lysocline. *Global Biogeochem. Cycles* **10**, 511–526.

Archer, D. and Maier-Reimer, E. 1994. Effect of deep-sea sedimentary calcite preservation on atmospheric CO_2 concentration. *Nature* **367**, 260–263.

Banse, K. 1982. Cell volumes, maximal growth rates of unicellular algae and ciliates, and the role of ciliates in the marine pelagial. *Limnol. Oceanogr.* **27**, 1059–1071.

Banse, K. 1992. Grazing, temporal changes of phytoplankton concentrations and the microbial loop in the open sea. In: *Primary Productivity and Biogeochemical Cycles in the Sea* (eds P. Falkowski and A. D. Woodhead). Plenum Press, New York, 409–439.

Barnes, R. S. K. and Hughes, R. N. 1988. *An Introduction to Marine Ecology*. Blackwell Science, Oxford.

Battle, M., Bender, M., Sowers, T., Tans, P. P., Butler, J. H. et al. 1996. Atmospheric gas concentrations over the past century measured in air from firn at the South Pole. *Nature* **383**, 231–235.

Berger, W. H., Fischer, K., Lai, C. and Wu, G. 1987. Ocean carbon flux: global maps of primary production and export production. In: *Biogeochemical Cycling and Fluxes Between the Deep Euphotic Zone and Other Realms* Research Report 88-1, NOAA Undersea Research Program (ed. C. R. Agegian). NOAA, Silver Spring, MD, 131–176.

Bopp, L., Monfray, P., Aumont, O., Dufresne, J. L., Le Treut, H. et al. 2001. Potential impact of climate change on marine export production. *Global Biogeochem. Cycles* **15**, 81–99.

Brewer, P. G. 2000. Gas hydrates: challenges for the future. *Ann. N. Y. Acad. Sci.* **912**, 195–199.

Broecker, W. S. 1991. Keeping global change honest. *Global Biogeochem. Cycles* **5**, 191–192.

Broecker, W. S. and Peng, T.-H. 1982. *Tracers in the Sea*. Lamont-Doherty Geological Observatory, New York.

Broecker, W. S. and Peng, T.-H. 1993. *Greenhouse Puzzles: Keeling's World; Archer's World; Walker's World*. Lamont-Doherty Earth Observatory, New York.

Copin-Montegut, C. and Copin-Montegut, G. 1983. Stoichiometry of carbon, nitrogen and phosphorus in marine particulate matter. *Deep-Sea Res.* **30**, 31–46.

Cornell, S., Rendell, A. and Jickells, T. 1995. Atmospheric inputs of dissolved organic nitrogen to the oceans. *Nature* **376**, 243–246.

Cox, P. M., Betts, R. A., Jones, C. D., Spall, S. A. and Totterdell, I. J. 2000. Acceleration of global warming due to carbon-cycle feedbacks in a coupled climate model. *Nature* **408**, 184–187.

Craig, H. 1957. The natural distribution of radiocarbon and the exchange time of carbon dioxide between atmosphere and sea. *Tellus* **9**, 1–17.

Craig, H., Broecker, W. S. and Spencer, D. 1981. *GEOSECS Pacific Expedition: Volume 4, Sections and Profiles*. US Government Printing Office, Washington, DC.

Dace, R. A., Liss, P. S., Merril, J. T., Aflas, E. L., Buat-Menard, P. and co-authors. 1991. The atmospheric input of trace species to the world ocean. *Globol Biogeochem. Cycles* **5**, 193–259.

Davies, A. G. and Sleep, J. A. 1981. The photosynthetic response of nutrient-depleted dilute cultures of *Skeletonema costatum* to pulses of ammonium and nitrate; the importance of phosphate. *J. Plankton Res.* **11**, 141–164.

Enting, I. G., Wigley, T. M. L. and Heimann, M. 1994. *Future Emissions and Concentrations of Carbon Dioxide: Key Ocean/Atmosphere/Land Analyses*. CSIRO Division of Atmospheric Research, Victoria.

Friedlingstein, P., Dufresne, J. L., Cox, P. M. and Rayner, P. 2003. How positive is the feedback between climate change and the carbon cycle? *Tellus* **55B**, 692–700.

Frost, B. W. and Franzen, N. C. 1992. Grazing and iron limitation in the control of phytoplankton stock and nutrient concentration—a chemostat analog of the pacific equatorial upwelling zone. *Mar. Ecol. Progr. Ser.* **83**, 291–303.

Furnas, M., J. 1990. *In situ* growth rates of marine phytoplankton: approaches to measurement, community and species growth rates. *J. Plankton Res.* **12**, 1117–1151.

Gattuso, J.-P., Frankignoulle, M., Bourge, I., Romaine, S. and Buddemeier, R. W. 1998. Effect of calcium carbonate saturation of seawater on coral calcification. *Global Planet. Change* **18**, 37–46.

Goldman, J. C. and Glibert, P. M. 1983. Kinetics of inorganic nitrogen uptake by phytoplankton. In: *Nitrogen in the Marine Environment* (eds E. J. Carpenter and D. G. Capone. Academic Press, New York, 233–274.

Gruber, N. and Keeling, C. D. 2001. An improved estimate of the isotopic air–sea disequilibrium of CO_2: implications for the oceanic uptake of anthropogenic CO_2. *Geophys. Res. Lett.* **28**, 555–558.

Holligan, P. M. and Robertson, J. E. 1996. Significance of ocean carbonate budgets for the global carbon cycle. *Global Change Biol.* **2**, 85–95.

IPCC 2001. *Climate Change 2001: The Scientific Basis. Contribution of Working Group I to the Third Assessment Report of the Intergovernmental Panel on Climate Change*. Cambridge University Press, Cambridge.

Jaffe, D. A. 1992. The nitrogen cycle. In: *Global Biogeochemical Cycles* (eds S. S. Butcher, R. J. Charlson, G. O. Orians and G. V. Wilde). Academic Press, New York, 263–284.

Jahnke, R. A. 1992. The phosphorus cycle. In: *Global Biogeochemical Cycles* (eds S. S. Butcher, R. J. Charlson, G. O. Orians and G. V. Wilde). Academic Press, New York, 301–315.

Johns, T. C., Gregory, J. M., Ingram, W. J., Johnson, C. E., Jones, A. et al. 2003. Anthropogenic climate change for 1860 to 2100 simulated with the HadCM3 model under updated emissions scenarios. *Clim. Dyn.* **20**(6), 583–612, doi:10.1007/s00382-002-0296-y.

Joos, F., Plattner, G.-K., Stocker, T. F., Marchal, O. and Schmitter, A. 1999. Global warming and marine carbon cycle feedbacks on future atmospheric CO_2. *Science* **284**, 464–467.

Keeling, R. F., Piper, S. C. and Heimann, M. 1996. Global and hemispheric CO_2 sinks deduced from changes in atmospheric O_2 concentration. *Nature* **381**, 218–221.

Khesghi, H. S., Flannery, B. P. and Hoffert, M. I. 1991. Marine biota effects on the compositional structure of the world oceans. *J. Geophys. Res.* **89**, 4957–4969.

Klepper, O. and de Haan, B., J. 1995. A sensitivity study of the effect of global change on ocean carbon uptake. *Tellus* **47B**, 490–500.

Kleypas, J. A., Buddemeier, R. W., Archer, D., Gattuso, J.-P., Langdon, C. et al. 1999. Geochemical consequences of increased atmospheric carbon dioxide on coral reefs. *Science* **284**, 118–120.

Langdon, C., Takahashi, T., Sweeney, C., Chipman, D., Goddard, J. et al. 2000. Effect of calcium carbonate saturation state on the calcification rate of an experimental coral reef. *Global Biogeochem. Cycles* **14**, 639–654.

Levitus, S. 1982. *Climatological Atlas of the World Ocean*. US Government Printing Office, Washington, DC.

Lewis, E. and Wallace, D. 1997. Documentation of program CO2SYS. In: *Inorganic Carbon for the World Ocean Circulation Experiment—World Hydrographic Program*. US Department of Energy Office of Health and Environmental Research, Oak Ridge, TN.

Libes, S. M. 1992. *An Introduction to Marine Biogeochemistry*. John Wiley, New York.

Lomas, M. W., Bates, N. R., Knap, A. H., Karl, D. M., Lukas, R. et al. 2002. Refining our understanding of oceanic biogeochemistry and ecosystem functioning. *EOS, Trans. Am. Geophys. Un.* **83**, 559–567.

Longhurst, A. R. 1991. A reply to Broecker's charges. *Global Biogeochem. Cycles* **5**, 315–316.

Ludwig, W., Amiotte-Suchet, P. and Probst, J.-L. 1996. River discharges of carbon to the world's oceans: determining local inputs of alkalinity and of dissolved and particulate organic carbon. *C. R. Acad. Sci. Ser. IIa* **323**, 1007–1014.

Mackenzie, F. T., Ver, L. M., Sabine, C., Lane, M. and Lerman, A. 1993. C, N, P and S global biogeochemical cycles and modeling of global change. In: *Interactions of C, N, P and S Biogeochemical Cycles and Global Change*, NATO ASI Series 14 (eds R. Wollast, F. T. Mackenzie and L. Chou), Springer, Berlin, 521.

Maier-Reimer, E., Mikolajewicz, U. and Hasselman, K. 1993. Mean circulation of the Hamburg LSG OGCM and its sensitivity to the thermohaline surface forcing. *J. Phys. Oceanogr.* **23**, 731–757.

Maier-Reimer, E., Mikolajewicz, U. and Winguth, A. 1996. Future ocean uptake of CO_2 interaction between ocean circulation and biology. *Clim. Dyn.* **12**, 711–721.

Martin, J. H., Knauer, G. A., Karl, D. M. and Broenkow, W. W. 1987. VERTEX: carbon cycling in the northeast Pacific. *Deep-Sea Res.* **34**, 267–285.

Matear, R. J. and Hirst, A. C. 1999. Climate change feedback on the future oceanic CO_2 uptake. *Tellus* **51B**, 722–733.

McAllister, C. D., Shah, N. and Strichland, J. D. H. 1964. Marine phytoplankton photosynthesis as a function of light intensity: a comparison of methods. *J. Fish. Res. Board Can.* **21**, 159–181.

Meybeck, M. 1993. C, N, P and S in rivers: from sources to global inputs. In: *Interactions of C, N, P and S Biogeochemical Cycles and Global Change*, NATO ASI Series, 14, (eds R. Wollast, F. T. Mackenzie and L. Chou). Springer, Berlin, 163–195.

Mikolajewicz, U., Santer, B. D. and Maier-Reimer, E. 1990. Ocean response to greenhouse warming. *Nature* **345**, 589–593.

Milliman, J. D. 1993. Production and accumulation of calcium carbonate in the ocean; budget of a nonsteady state. *Global Biogeochem. Cycles* **7**, 927–957.

Milliman, J. D., Troy, P. J., Balch, W. M., Adams, A. K., Li, Y.-H. and coauthors 1999. Biologically mediated dissolution of calcium carbonate above the chemical lysocline? *Deep-Sea Res. I* **46**, 1653–1669.

Morse, J. W. and Mackenzie, F. T. 1990. *Geochemistry of Sedimentary Carbonates*. Amsterdam, Elsevier.

Munk, W. H. 1966. Abyssal recipes. *Deep-Sea Res.* **13**, 707–730.

Oreskes, N., Shrader-Frechette, K. and Belitz, K. 1994. Verification, validation, and confirmation of numerical models in the earth sciences. *Science* **263**, 641–646.

Orr, J. C., Maier-Reimer, E., Mikolajewicz, U., Monfray, P., Sarmiento, J. L. et al. 2001. Estimates of anthropogenic carbon uptake from four three-dimensional global models. *Global Biogeochem. Cycles* **15**, 43–60.

Palmer, J. R. and Totterdell, I. J. 2001. Production and export in a global ocean ecosytem model. *Deep-Sea Res. I* **48**, 1169–1198.

Plattner, G.-K., Joos, F., Stocker, T. F. and Marchal, O. 2001. Feedback mechanisms and sensitivities of ocean carbon uptake under global warming. *Tellus* **53B**, 564–592.

Prentice, I. C., Farquhar, G. D., Fasham, M. J. R., Goulden, M. L., Heimann, M. et al. 2001. The carbon cycle and atmospheric CO_2. In: *Climate Change 2001: The Scientific Basis* (eds J. T. Houghton, Y. Ding, D. J. Gripggs, M. Noguer, P. J. van der Linden and D. Xiaosu). Cambridge University Press, Cambridge, 944.

Press, W. H., Teukolsky, S. A., Vetterling, W. T. and Flannery, B. P. 1992. *Numerical Recipes in FORTRAN*. Cambridge University Press, Cambridge.

Riebesell, U., Zondervan, I., Rost, B., Tortell, P. D., Zeebe, R. E. et al. 2000. Reduced calcification of marine plankton in response to increased atmospheric CO_2. *Nature* **407**, 364–367.

Sarmiento, J. L. 1991. Oceanic uptake of anthropogenic CO_2: the major uncertainties. *Global Biogeochem. Cycles* **5**, 315–316.

Sarmiento, J. L. 1992. Biogeochemical ocean models. In: *Climate System Modelling* (ed. K. E. Trenbarth) Cambridge University Press, Cambridge, 511–549.

Sarmiento, J. L., Dunne, J., Gnanadesikan, A., Key, R. M., Matsumoto, K. et al. 2001. A new estimate of the CaCO3 to organic carbon export ratio. *Global Biogeochem. Cycles* **16**, doi:10.1029/2002GB001919.

Sarmiento, J. L., Huges, T. M. C., Stouffer, R. J. and Manabe, S. 1998. Simulated response of the ocean carbon cycle to anthropogenic climate warming. *Nature* **393**, 245–249.

Sarmiento, J. L. and Le Quéré, C. 1996. Oceanic carbon dioxide uptake in a model of century-scale global warming. *Science* **274**, 1346–1350.

Sarmiento, J. L., Orr, J. C. and Siegenthaler, U. 1992. A perturbation simulation of CO_2 uptake in an ocean general circulation model. *J. Geophys. Res.* **97**, 3621–3636.

Schlesinger, W. H. 1997. *Biogeochemistry: an Analysis of Global Change*. Academic Press, San Diego, CA.

Schlitzer, R. 1996. Global ocean export production and particle fluxes based on oxygen, nutrient and carbon data. *AGU Fall Meeting, San Francisco, Abstracts*. American Geophysical Union, Washington, DC.

Shaffer, G. 1993. Effects of the marine biota on global carbon cycling. In: *The global carbon cycle* (ed. M. Heimann). Springer, Berlin Heidelberg.

Shaffer, G. and Sarmiento, J. L. 1995. Biogeochemical cycling in the global ocean. 1. A new, analytical model with continuous vertical resolution and high-latitude dynamics. *J. Geophys. Res.* **100**, 2659–2672.

Siegenthaler, U. 1983. Uptake of excess CO_2 by an outcrop-diffusion model of the ocean. *J. Geophys. Res.* **88**, 3599–3608.

Siegenthaler, U. and Joos, F. 1992. Use of a simple model for studying oceanic tracer distributions of the global carbon cycle. *Tellus* **44B**, 186–207.

Siegenthaler, U. and Sarmiento, J. L. 1993. Atmospheric carbon dioxide and the ocean. *Nature* **365**, 119–125.

Steele, J. H. and Henderson, E. W. 1992. The role of predation in plankton models. *J. Plankton Res.* **14**, 157–172.

Sundquist, E. T. 1985. Geological perspectives on carbon dioxide and the carbon cycle. In: *The Carbon Cycle and Atmospheric CO_2: Natural Variations, Archean to Present*, American Geophysical Union Monograph 32 (eds W. S. Broecker and E. T. Sundquist). American Geophysical Union, Washington, DC, 5–59.

Sundquist, E. T. 1986. Geologic analogs: their value and limitations in carbon dioxide research. In: *The Changing Carbon Cycle* (eds J. R. Trabalka and D. E. Reichle) Springer, New York, 371–403.

Takahashi, T., Broecker, W. S. and Bainbridge, A. E. 1981. Supplement to the alkalinity and total carbon dioxide concentration in the world oceans. In: *Carbon Cycle Modelling, SCOPE 16* (ed. B. Bolin). John Wiley, Chichester, 159–201.

Tyrrell, T. 1999. The relative influences of nitrogen and phosphorus on oceanic primary production. *Nature* **400**, 525–531.

Watson, A. J., Upstill-Goddard, R. C. and Liss, P. S. 1991. Air–sea gas exchange in rough and stormy seas measured by a dual-tracer technique. *Nature* **349**, 145–147.

Watson, R. T., Rodhe, H., Oeschger, H. and Siegenthaler, U. 1990. Greenhouse gases and aerosols. In: *Climate Change—the IPCC Scientific Assessment* (eds J. T. Houghton, G. J. Jenkins and J. J. Ephruams). Cambridge University Press, Cambridge, 1–40.

Wollast, R. 1994. The relative importance of biomineralization and dissolution of $CaCO_3$ in the global carbon cycle. *Bull. Inst. Oceanogr. Monaco* **13**, 13–35.

Yamanaka, Y. 1995. Study of the oceanic carbon cycle using an ocean biogeochemical general circulation model. In: *Proceedings of the Tsukuba Global Carbon Cycle Workshop* (ed. T. Matsuno) National Institute for Environmental Studies, Tsukuba, 65–66.

Yamanaka, Y. and Tajika, E. 1996. The role of the vertical fluxes of particulate organic matter and calcite in the oceanic carbon cycle: studies using an ocean biogeochemical general circulation model. *Global Biogeochem. Cycles* **10**, 361–382.